

Nonreciprocal interactions give rise to fast cilium synchronisation in finite systems

David J Hickey^a, Ramin Golestanian^{a,b,1}, and Andrej Vilfan^{a,c,1}

^aMax Planck Institute for Dynamics and Self-Organization (MPI-DS), 37077 Göttingen, Germany; ^bRudolf Peierls Centre for Theoretical Physics, University of Oxford, Oxford OX1 3PU, United Kingdom; ^cJožef Stefan Institute, 1000 Ljubljana, Slovenia

This manuscript was compiled on May 16, 2023

Motile cilia beat in an asymmetric fashion in order to propel the surrounding fluid. When many cilia are located on a surface, their beating can synchronise such that their phases form metachronal waves. Here, we computationally study a model where each cilium is represented as a spherical particle, moving along a tilted trajectory with a position-dependent active driving force and a position-dependent internal drag coefficient. The model thus takes into account all the essential broken symmetries of the ciliary beat. We show that taking into account the near-field hydrodynamic interactions, the effective coupling between cilia can become nonreciprocal: the phase of a cilium is more strongly affected by an adjacent cilium on one side than by a cilium at the same distance in the opposite direction. As a result, synchronisation starts from a seed at the edge of a group of cilia and propagates rapidly across the system, leading to a synchronisation time that scales proportionally to the linear dimension of the system. We show that a ciliary carpet is characterised by three different velocities: the velocity of fluid transport, the phase velocity of metachronal waves and the group velocity of order propagation. Unlike in systems with reciprocal coupling, boundary effects are not detrimental for synchronisation, but rather enable the formation of the initial seed.

Cilia | Low Reynolds number hydrodynamics | Metachronal waves | Nonreciprocal interactions

Motile cilia are hairlike organelles which can move under their own power in order to fulfil roles such as fluid pumping or mixing (1). They are nigh-ubiquitous in biological systems, being found on most eukaryotic cells (2) including in the nervous system (3), the respiratory system (4), and the olfactory system (5). This makes them central to many open questions in biology, such as the precise mechanism behind the emergence of left-right differentiation during embryonic development (6). While the fascinating fluid dynamical questions involved in the dynamics of cilia and their biological function have been already highlighted by the pioneers of twentieth century fluid dynamics, such as Ludwig Prandtl (7) and G. I. Taylor (8), the subject of the collective properties of hydrodynamically active organelles at low Reynolds number continues to be an active field of research, particularly as a key component of the field of active matter (9).

When many motile cilia are located on a surface at sufficient density, their beating can synchronise with a phase lag between neighbouring cilia. The resulting phase waves are called metachronal waves. It has been shown that metachronal coordination can lead to a high energetic efficiency of swimming or fluid transport (10, 11), and that metachronal waves may reduce collisions between cilia, further raising pumping speed (12). Moreover, the coordination has been shown to be beneficial for the efficiency of the chemosensory function of motile cilia (13). Metachronal waves are found in many

different organisms and systems. For example, *Paramecium* uses metachronally coordinated cilia to swim (14), as well as to feed (14). Indeed, *Paramecium*'s swimming efficiency is close to the maximum possible efficiency for an organism with cilia of that length (10). Metachronal waves are found in other systems, such as the multicellular colony *Volvox* (15) or cilia in the respiratory tract (4) where their pumping efficiency is important for moving mucus (16). Metachronal coordination also appears in animals (e.g., krill) at larger length scales with very different coordination mechanisms (17).

Metachronal waves can be classified according to the direction of the wave propagation, depending on how the phase velocity of the wave compares to the direction of fluid transport. When these two directions are parallel, the metachronal wave is said to be symplectic. If they are antiparallel, the wave is called antiplectic (18). Other wave directions are classified as dextiolectic or leoplectic.

The fact that a pair of hydrodynamically interacting cilia or flagella can synchronise their cycles, even when belonging to two separate organisms (19), suggests that hydrodynamic coupling alone can be sufficient to explain the emergence of metachronal waves. Nevertheless, some studies also point to the additional role of intracellular linkages (20–22). In fact, the metachronal waves in *Paramecium* can preserve synchrony across the wall of a micropipette that isolates them hydrodynamically (23).

A fundamental problem in understanding synchronisation via hydrodynamic interactions is the reversible nature of the

Significance Statement

Motile cilia are hairlike organelles that, at sufficient density, can synchronise hydrodynamically with their neighbours to form a metachronal wave. We use a minimal model of a ciliary carpet that accounts for near-field hydrodynamic coupling between cilia and show that the interaction between cilia can be nonreciprocal. We propose to characterize the collective dynamics of an array of cilia by three different velocities and their directions: the direction of fluid transport, the direction of metachronal waves (phase velocity) and the direction of order propagation (group velocity). The latter determines the time scale of synchronization. Near-field nonreciprocal interactions can therefore give rise to rapid emergence of metachronal waves.

R.G. and A.V. designed research; D.J.H. performed research; D.J.H. and A.V. analyzed data; D.J.H., R.G. and A.V. wrote the paper.

The authors declare no competing interests.

¹To whom correspondence should be addressed. E-mail: ramin.golestanian@ds.mpg.de, andrej.vilfan@ds.mpg.de

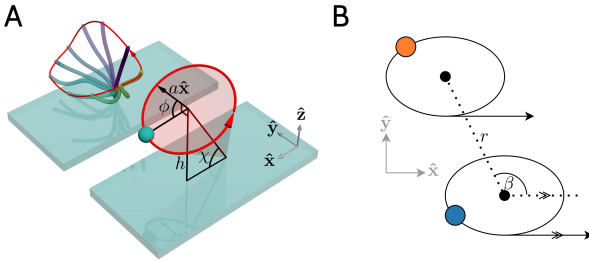


Fig. 1. Illustration of the model, showing the parameters used. (A) A realistic cilium motion with the trajectory shown in red. The power stroke (solid blue colour) gives way to a slower recovery stroke along the no-slip surface of the substrate, resulting in net fluid flow in the direction of the power stroke over a cycle. Also shown is one of our model cilia that approximates the realistic motion, with the trajectory shown in red, and relevant quantities indicated. The circular trajectory retains the essential features of a power stroke far from the substrate and a recovery stroke much closer. (B) Definition of β and the intercilium distance r . The arrows represent the direction of the power stroke of the cilium, occurring at the highest point above the surface. Feathering on lines indicates that they are parallel, so that β is the angle between the power stroke and the displacement vector connecting the lattice points of two cilia.

55 Stokesian hydrodynamics, i.e. the fact that the fluid flow
 56 exactly reverses its direction upon the reversal of actuating forces, whereas the tendency of a system to reach an ordered
 57 state is by definition irreversible (9). Theoretical models
 58 therefore have to take into account higher order effects that
 59 break the respective symmetries. These can include a second
 60 degree of freedom per cilium (24–29), the asymmetric spatial
 61 arrangement of cilia (30), a trajectory or driving force with
 62 sufficiently broken symmetries (28, 31–37), or a non-linear
 63 driving mechanism that, for instance, switches the direction
 64 of force when a switch point is reached (11, 38–41).

65 When discussing the role of symmetries for ciliary synchronisation, one has to keep in mind that reciprocity manifests
 66 itself differently for conservative or dissipative interactions.
 67 For conservative forces, Newton's third law states that opposite forces are exerted on both interacting bodies. For
 68 hydrodynamic interactions, which are dissipative in their nature,
 69 the Lorentz reciprocal theorem (42) implies that the force on one body, caused by the motion of a second one with
 70 a given velocity, is identical to the force on the second body when the first body moves with the same velocity. Hydrodynamic interactions therefore act on both bodies with the same sign. The interplay of both interaction types is one possibility to facilitate ciliary synchronisation (26). In active systems, nonreciprocal interactions can arise where the effect of the interaction on body A differs from that on body B, both in magnitude and direction (33, 43–49). For example, in the Vicsek model, particles or animals can be affected by other particles in front of them in a different way from those behind them. The orientation of hydrodynamically coupled rotors is a prime example of nonreciprocal coupling that leads to a rich phenomenology, including turbulent behaviour via defect proliferation and annihilation (31).

88 A major open question is related to the scaling with the
 89 system size and the role of boundaries of the ciliated region.
 90 Recent theoretical work shows that the time needed to reach
 91 synchronisation scales quadratically with the number of cilia
 92 (50). In principle, the metachronal wave vector of the final state
 93 is not uniquely determined. However, the basins of attraction of
 94 different solutions can greatly differ in size, leading to a

95 strong preference for one state (50). Boundaries are often
 96 detrimental for synchronisation, because the cilia at the edge
 97 have a smaller number of nearest neighbours, which can affect
 98 their characteristic frequency, as demonstrated in a small
 99 1D row of artificial oscillators (51). Boundary effects in a
 100 finite system can even lead to the emergence of a chimera
 101 state in which the oscillators split up into a coherent and an
 102 incoherent population (52). The vast majority of theoretical
 103 and computational studies focus on systems with periodic
 104 boundary conditions as a representation of generic, infinite
 105 systems (11, 26, 31, 32, 34, 38, 50, 53, 54). In nature, periodic
 106 circular 1D chains of cilia exist, for instance the oral cilia of
 107 *Stentor* (55) or in starfish larvae (56). However, for topological
 108 reasons 2D arrangements of cilia need open boundaries or
 109 topological defects, as it is impossible to have a polar field on
 110 the topology of a sphere without discontinuities.

111 In this paper, we show that the near-field effects between
 112 hydrodynamically coupled cilia can lead to an effective non-
 113 reciprocal interaction, where cilium A can affect the phase of
 114 cilium B more strongly than vice versa. As a result of this
 115 nonreciprocity, the metachronal order propagates through the
 116 array of cilia with a group velocity, which is not directly re-
 117 lated to the velocity of the fluid transport or the phase velocity
 118 of metachronal waves. In a finite group of cilia, order then
 119 emerges at a boundary and propagates across the group in a
 120 time that scales linearly with the system dimension, an order
 121 of magnitude faster than an equivalent system without near-
 122 field hydrodynamics. We suggest that nonreciprocal coupling
 123 is key to understanding the fast emergence of synchronisation
 124 in large ciliary carpets. The dynamics of the tissue are then
 125 characterised by three independent velocities: the velocity
 126 of fluid transport above the surface, the phase velocity of
 127 metachronal waves, and the group velocity with which the
 128 order propagates.

Results. Cilia are long and thin, and beat with a time-irreversible whip-like stroke (1). Because of the complexity of the cilium stroke, its description quickly leads to an intractable number of parameters. We therefore take a simplified approach common to many theoretical models (e.g., 30, 34, 35) and replace the cilium with a small sphere, pushed along a fixed trajectory by a position-dependent active force. The position of the sphere represents the tip position of a cilium and the active driving force represents the activity of dynein motors of the cilium's axoneme. We thus consider a sphere of radius b moving on a fixed circular trajectory of radius a , with its centre a distance h above a surface. The sphere is driven by an internal driving force $F^{\text{dr}}(\phi)$ and has an internal friction coefficient $\Gamma(\phi)$, both of which act in the tangential direction of the trajectory. The tilt of the trajectory is controlled by an angle χ such that when $\chi = \pi/2$, the trajectory lies in a plane parallel to the substrate beneath the cilium, shown in Fig. 1A.

This choice to model the cilia as single spheres on fixed tilted circular trajectories means that we neglect much of the fluid flow driven by the cilium closer to the surface, while preserving the irreversibility of the cilium beat – essential given the inherent irreversibility of synchronisation. This approximation also replicates the pumping ability of the cilium: when the cilium is closer to the no-slip surface, it produces less fluid flow, and when it is further away it produces more. Over a cycle, the cilium moves a positive net amount of fluid in the direction of its 'power stroke'. At distances from the cilium

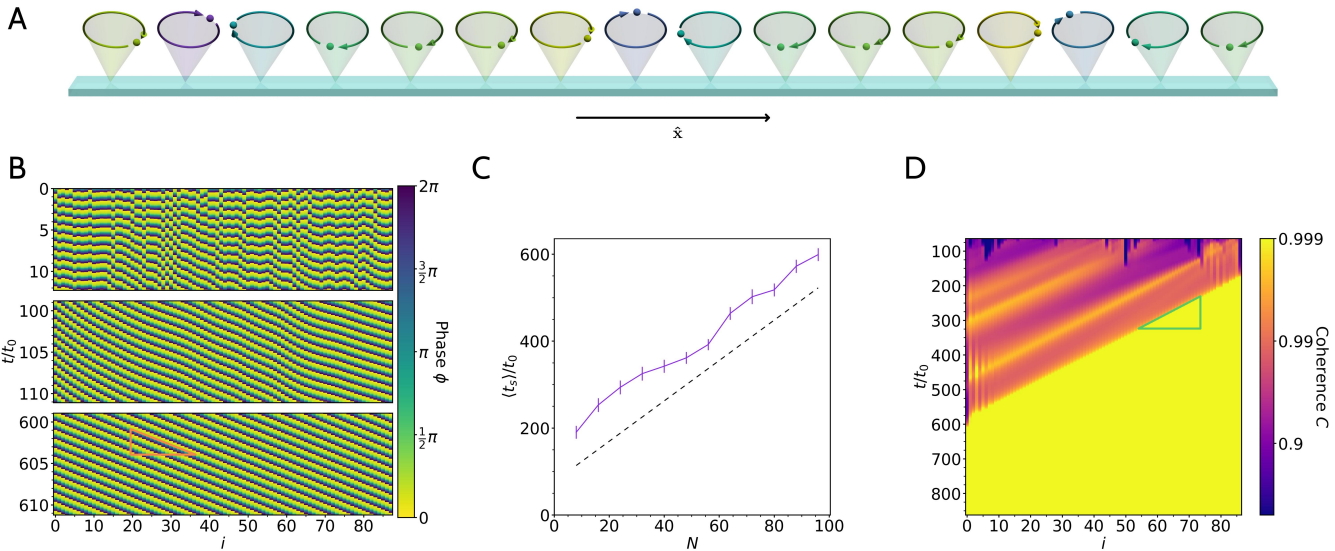


Fig. 2. Synchronisation in a one-dimensional row of cilia. (A) A snapshot from the simulation. The colours indicate the phases. (B) A kymograph showing the metachronal waves in the system at different times. The simulation starts with random phases, but patches of order quickly assert themselves and give rise to waves that are initially uneven but eventually become completely uniform. The waves travel with the phase velocity v_{ph} (orange triangle) in the direction of fluid transport, and are hence symplectic waves. (C) The mean synchronisation time $\langle t_s \rangle$ vs. the number of cilia N . The mean is calculated by simulating many systems at each size with different random initial phase configurations, and measuring how long it takes to synchronise using a metric based on standard deviation of cilium frequencies. The figure shows that the synchronisation time scales approximately linearly in the system size. Error bars are standard error of the mean, based on ≥ 92 simulations. (D) A kymograph showing the coherence between adjacent pairs of cilia. On this graph each value of i on the abscissa corresponds to the coherence between cilium i and $i + 1$. Once an ordered patch forms on the right edge it spreads across the row with the group velocity v_g (green triangle) in the negative x direction. The fact that the synchronisation time is mainly limited by the propagation across the system explains the linear size-dependence in panel (C).

that are several times greater than h , this approximation gives almost identical fluid flow to a more detailed treatment of the cilium (57). In the following, we orient the pumping direction in the positive x -direction.

To study synchronisation and the emergence of metachronal waves, we now consider many cilia arranged on a two-dimensional surface. Each point $\mathbf{r}_i = (x_i, y_i, 0)$ represents the position on the substrate directly below the centre of a cilium's trajectory. A pair of cilia (i and j) is characterised by the angle β_{ij} , which is the angle between the working stroke of cilium i (along the x -axis, Fig. 1) and the line pointing from \mathbf{r}_i to \mathbf{r}_j . These quantities are illustrated in Fig. 1B.

The position \mathbf{R}_i of the sphere representing cilium i is parameterised as a function of its phase ϕ_i following the notation used by Meng et al. (34):

$$\mathbf{R}_i(\phi_i) = \mathbf{r}_i + \begin{pmatrix} a \cos \phi_i \\ a \sin \phi_i \sin \chi \\ h - a \sin \phi_i \cos \chi \end{pmatrix}. \quad [1]$$

To replicate the beating cycle of a cilium, which consists of a fast working stroke followed by a slower sweeping recovery stroke, we introduce a position-dependent force and an internal drag coefficient, which together determine the force-velocity relationship of the active driving force $F^{dr}(\phi_i) - \Gamma(\phi_i)v$. Both can be expanded in a Fourier series as:

$$F^{dr}(\phi_i) = F_0^{dr} \left[1 + \sum_n^{\infty} A_n \cos(n\phi_i) + B_n \sin(n\phi_i) \right], \quad [2]$$

$$\Gamma(\phi_i) = \Gamma_0 \left[1 + \sum_n^{\infty} C_n \cos(n\phi_i) + D_n \sin(n\phi_i) \right]. \quad [3]$$

In the following, we only account for terms where $n \leq 2$. This simplification is justified, as the first harmonic is known to be essential for synchronisation (and indeed is well-placed to replicate the cilium's beating pattern of a fast power stroke and a slower recovery stroke) but the second harmonic is much more effective at driving the onset of synchronisation and ensuring a more stable synchronised state (28, 35, 36).

Due to the linearity of the Stokes flow, the hydrodynamic force \mathbf{F}_i^h on a particle is a linear function of the particle's own velocity and the velocities of all other particles it hydrodynamically interacts with. It can be expressed with a generalised friction tensor in the presence of a no-slip boundary, $\Gamma(\phi_i, \phi_j)$, as $\mathbf{F}_i^h = -\sum_j \Gamma(\phi_i, \phi_j) \cdot \mathbf{v}_j$. Along with the driving force, which is always tangential to the trajectory, and a perpendicular constraint force \mathbf{F}^{cstr} which keeps the particle on the trajectory, the force balance on cilium i states:

$$\mathbf{F}^{dr}(\phi_i) + \mathbf{F}^{cstr} - \Gamma(\phi_i)\mathbf{v}_i - \sum_j \Gamma(\phi_i, \phi_j) \cdot \mathbf{v}_j = 0. \quad [4]$$

By considering only its tangential component (i.e., multiplying the above equation with the tangent vector $\mathbf{t}(\phi_i)$), we obtain the equations of motion for each cilium:

$$\mathbf{F}^{dr}(\phi_i) = \Gamma(\phi_i)v_i + \sum_j \mathbf{t}(\phi_i) \cdot \Gamma(\phi_i, \phi_j) \cdot \mathbf{t}(\phi_j)v_j. \quad [5]$$

Here, the velocities are related to the phase derivatives as $\mathbf{v}_i = (\partial \mathbf{R}_i / \partial \phi_i)\phi_i$. By solving these equations numerically, we can simulate the evolution of the cilium phases ϕ_i over time. In the following, we non-dimensionalise all time units using the time period of an isolated cilium t_0 , which can

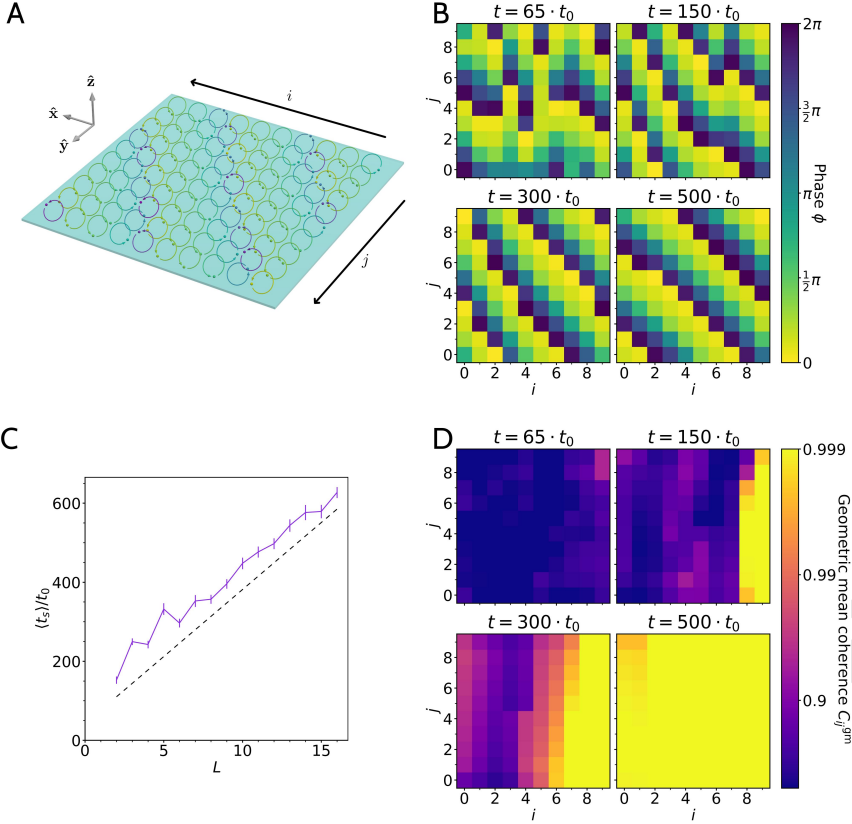


Fig. 3. Synchronisation in a two-dimensional square lattice. (A) A schematic of the simulation of the square $L \times L$ lattice at a synchronised state for the specific case $L = 10$. The colour of each model cilium indicates its phase, making the order clearly visible. See also Movie S1 for an animated representation. (B) A series of snapshots showing the phases of the cilia in the square lattice, for the specific case of $L = 10$ (see movie S2 for a complete time series). (C) The mean synchronisation time $\langle t_s \rangle$ vs. the linear dimension of the system L . The mean is calculated by simulating many systems at each size with different random initial phase configurations, and measuring how long it takes for the standard deviation of the cilium frequencies in each system to drop below a certain threshold value. The synchronisation time scales approximately linearly in L . Error bars are standard error of the mean, based on ≥ 31 samples. (D) The geometric mean of the coherence between each cilium and all of its neighbours for a specific simulation with $L = 10$. The order emerges on the right side and spreads across the system in negative x direction, leading to the observed linear dependence between the synchronisation time and the length L .

be determined as $t_0 = \int_0^{2\pi} (\dot{\phi}_i)^{-1} d\phi_i$ using Eq. (5) without interacting neighbours.

Symmetries. Before discussing the numerical solutions, it is instructive to consider the symmetries of the system and their effect on synchronisation and formation of metachronal waves. Our model contains the following symmetries:

- (i) Swapping. Because all cilia are intrinsically equal, the equations of motion stay the same when exchanging two cilia ($\phi_1 \leftrightarrow \phi_2$) and re-arranging them such that $\beta \leftrightarrow \beta + \pi$.
- (ii) Mirror symmetry. The trajectories of cilia (but not their drag and driving force) are symmetric with respect to $y \leftrightarrow -y$. The equations of motion therefore contain the symmetry $\beta \leftrightarrow \pi - \beta$, $\phi \leftrightarrow \pi - \phi$, $F_0^{\text{dr}} \leftrightarrow -F_0^{\text{dr}}$ with the adjustment of the coefficients defined in Eqs. (2, 3): $(A_n, C_n) \leftrightarrow (-1)^n (A_n, C_n)$ and $(B_n, D_n) \leftrightarrow -(-1)^n (B_n, D_n)$.
- (iii) Time reversal. Due to the time-reversibility of the Stokes equation, the equations of motion also remain invariant under the transformation $F_0^{\text{dr}} \leftrightarrow -F_0^{\text{dr}}$ and $t \rightarrow -t$. Because of the time-reversal, a solution that is stable in the original system becomes unstable in the transformed system.
- (iv) Without near-field hydrodynamics: axial reflection. If the distance between cilia is sufficient that the near-field hydrodynamic interactions can be neglected ($r \gg h$), the mobility tensor ($\mathbf{M} = \mathbf{\Gamma}^{-1}$) for two particles at a distance

$\Delta\mathbf{x} = (\Delta x, \Delta y, 0)$, where $\Delta x = x_j - x_i$ and $\Delta y = y_j - y_i$, can be approximated as (30)

$$\mathbf{M}(\mathbf{x}_i, \mathbf{x}_j) = \frac{3}{2\pi\eta} \cdot \frac{z_i z_j}{|\Delta\mathbf{x}|^5} \begin{pmatrix} (\Delta x)^2 & \Delta x \Delta y & 0 \\ \Delta y \Delta x & (\Delta y)^2 & 0 \\ 0 & 0 & 0 \end{pmatrix}. \quad [6]$$

At the same time, the variation of the horizontal positions (x, y) of a cilium during a cycle can be neglected such that the motion along the trajectory only affects the vertical distances z_i and z_j . The far-field mobility tensor is therefore symmetric with respect to $\beta \leftrightarrow \beta + \pi$.

The above symmetry properties have bold consequences for the synchronisation. Consider a row of cilia arranged along the x axis, in the direction of pumping. In such a row, the angles β can only have values 0 and π . Without any of the coefficients that change sign under (ii), i.e., A_1, C_1, B_2, \dots , the motion is symmetric upon the combination of transformations (i), (ii) and (iii). Because the combined transformation contains time reversal which renders a stable solution unstable, no stable states are possible under these assumptions. The notion is consistent with the result in (30) if two cilia are arranged along the pumping direction. The existence of a stable solution requires at least one of the terms $A_1, C_1, B_2, D_2, A_3, C_3$, etc. to be nonzero. The same argument also holds for a row of cilia arranged along the y axis (perpendicular to the pumping direction) when the symmetries (ii) and (iii) are employed (see related arguments in (9, 58)).

Without near-field effects (NFEs) in the hydrodynamic coupling, the symmetry property (iv) immediately implies the equivalence of metachronal waves with wave vectors \mathbf{k} and

– \mathbf{k} , as seen in (34). We therefore expect such systems to show the emergence of multiple long-lived domains with different metachronal wave vectors.

Near-field effects in combination with (for instance) the rotational motion of cilia can break the spatial symmetry, and lead to antisymmetric coupling terms that synchronise the cilia into a state with a non-zero phase difference (9, 30, 58–60). Here, we point out that the interactions are not only asymmetric with respect to the phase difference, but also nonreciprocal with respect to their strength. In a given configuration, the response of cilium i to the phase of cilium j can differ from the response of cilium j to cilium i both in the magnitude and in the phase dependence. This nonreciprocity has profound implications for the emergence of metachronal waves.

Synchronisation in one dimension. We first consider a one-dimensional row of cilia with uniform spacing d and open boundaries such that cilium i is located at position $\mathbf{r}_i = (id, 0, 0)$ (see Fig. 2A). This means that $\beta_{ij} = 0$ or π for every cilium pair $i \neq j$. We used numerical simulations to see how order emerged in the system when the cilia were initialised with random initial phases.

Figure 1B shows the phases of the cilia on a kymograph. The initially random phases quickly coalesce into mostly ordered waves, which slowly become more ordered over time until the waves are completely uniform. The average time t_s to reach a synchronised state scales approximately linearly with the system length (Fig. 1C). We consider the state as synchronised when the standard deviation of all cilium frequencies falls below a fixed threshold. The linear dependence can be understood by looking at the signal coherence between adjacent pairs of cilia (Fig. 1D). The signal coherence is a measure of the degree of linear dependence between two signals, given as a function of the frequency, with values between 0 and 1. For two signals in the time domain $x(t)$ and $x'(t)$, the coherence is calculated as

$$C_{xx'}(f) = \frac{|\tilde{x}^*(f)\tilde{x}'(f)|^2}{\tilde{x}(f)\tilde{x}'(f)}, \quad [7]$$

where $\tilde{x}(f)$ and $\tilde{x}'(f)$ indicate the Fourier transforms of $x(t)$ and $x'(t)$, respectively. For every pair of cilia, we calculate the coherence between $\cos(\phi_i(t))$ and $\cos(\phi_j(t))$ at the frequency with the strongest cross-spectral density between the two signals (i.e., the frequency f that maximises the numerator in Eq. (7)).

Random patches of order sometimes emerge and travel against the pumping direction (in this case the pumping direction is rightwards), as the nonreciprocal nature of the hydrodynamic interactions causes the order to expand on one side and be extinguished by the disorder on its other side. However, when an ordered patch occurs close enough to the rightmost edge, there is no disorder to its right to extinguish it, so it spreads throughout the system. This explains why we see that the synchronisation time has a roughly affine relationship with the system length.

Synchronisation in two dimensions. The vast majority of motile cilia are found in two-dimensional bundles on multiciliated cells, where the cells themselves are sparsely distributed (61). Hence, we consider a two-dimensional square lattice with side length L and lattice constant d (so that the total number

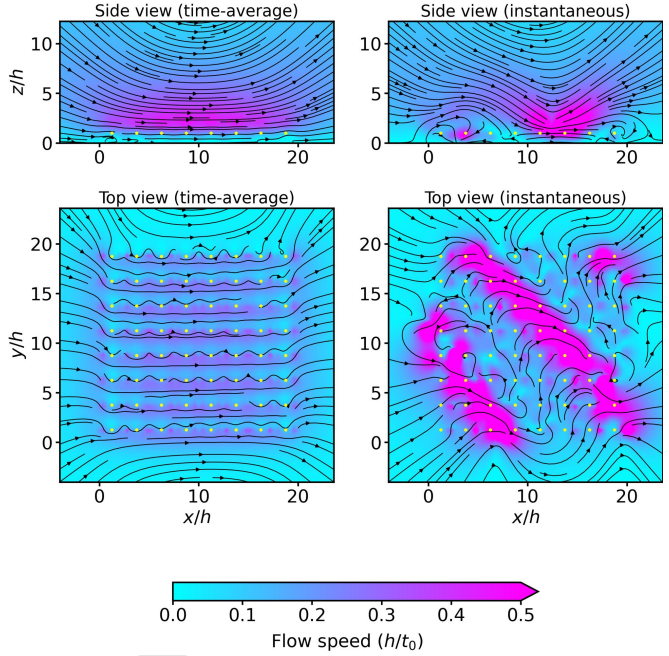


Fig. 4. Time-averaged and instantaneous flow in a system of 8×8 cilia after reaching a synchronised metachronal state. The background colour indicates the flow speed in units of h/t_0 and the yellow dots represent the centre of cilium orbits. The side view corresponds to a vertical cross-section through the middle of the array of cilia ($x/h = 10$) and the top view to a slice at $z = h$. The structure of the metachronal wave is clearly visible in the instantaneous flow fields.

of cilia is $N = L \times L$). We enforce open boundaries, and run a very similar simulation to the one described in the previous section. Figure 3A shows the lattice, with the cilium trajectories marked according to their phase, rendering the structure of the metachronal wave clearly visible. Figure 3B shows how the order of the cilia emerges over time: initially there is no correlation between phases, but over time some order emerges, which eventually solidifies into well-ordered metachronal waves.

Figure 3C shows that the synchronisation time scales approximately linearly with the linear dimension of the system L (i.e. $\langle t_s \rangle \sim L \sim \sqrt{N}$), just as in the one-dimensional case. This is explained by Fig. 3D, which illustrates the coherence of each cilium with its neighbours. For each cilium i the value is given by the geometric mean of coherence values with all directly adjacent (not including diagonally adjacent) cilia:

$$C_i^{\text{gm}} = \left[\prod_{j \in \{\text{n.n.}\}} C(\{\phi_i\}, \{\phi_j\}) \right]^{(1/N_{\text{n.n.}})}, \quad [8]$$

where $C(\{\phi\}, \{\phi'\})$ is the coherence, defined over two time series of phases. The resulting graph explains the linearity: the order emerges along one edge and gradually spreads across the entire lattice. Since the limiting factor to synchronisation is the time taken for the order to spread through the length of the system, this time depends on the linear dimension as L/v_g .

The flow field induced by a carpet of cilia that has reached the synchronised state with steady metachronal waves is shown in Figure 4. The time-averaged flows show a region of largely homogeneous flow above the carpet where the fluid is pumped

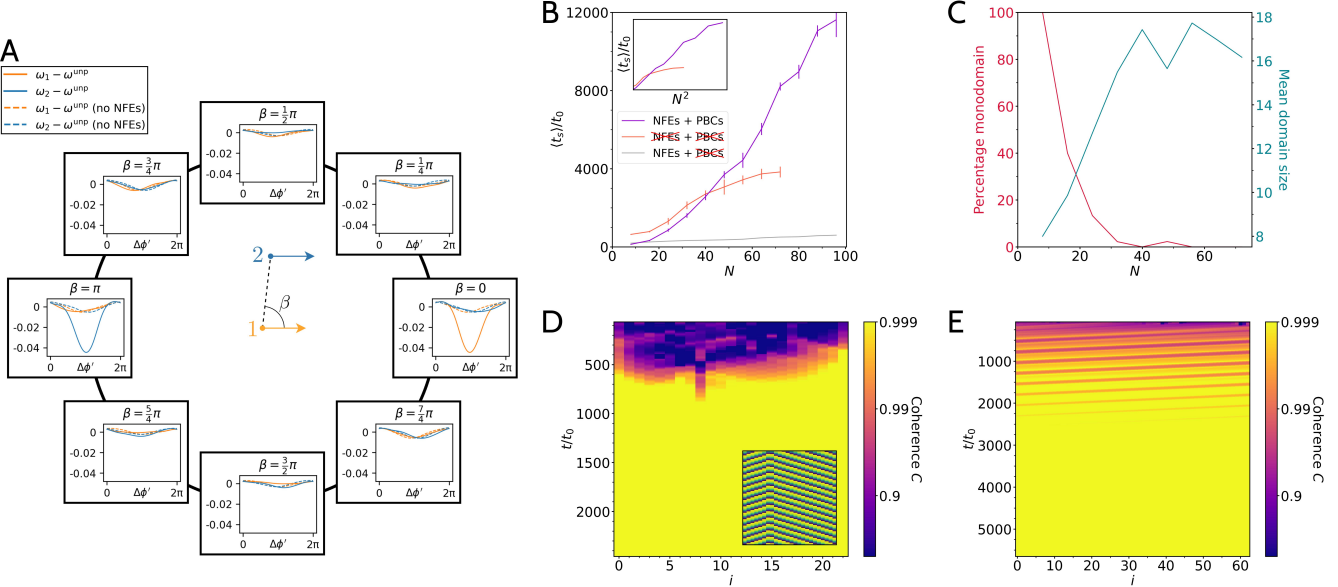


Fig. 5. The role of nonreciprocal hydrodynamic interactions and near-field effects in synchronisation. (A) The effective angular frequencies ω_1 and ω_2 of two interacting cilia (in dimensionless units) as a function of the adjusted difference $\Delta\phi'$. The cilia are positioned at a fixed distance ($r = 2.5h$) in different directions β . When the cilia are arranged in the x -direction ($\beta = 0, \pi$) there is a stark difference between ω_1 and ω_2 , showing that the interaction is highly nonreciprocal. The nonreciprocity is much weaker when the cilia are arranged y direction ($\beta = \pi/2$), and the nonreciprocity vanishes entirely when near-field hydrodynamic effects are disabled (dashed lines). (B) The mean time to reach the synchronised state $\langle t_s \rangle$ in a 1D row of N cilia with near-field effects disabled (orange) and with periodic boundary conditions (magenta). The synchronisation time is dramatically longer in both of these cases than in the one-dimensional open boundary case (grey line, data from Fig. 2C). The inset indicates that the scaling of these synchronisation times is close to $\langle t_s \rangle \sim N^2$. With open boundaries and no near-field effects, however, the synchronisation time reaches a plateau when the final state consists of multiple domains with different wave vectors. Error bars are standard error of the mean, based on 9 samples for the periodic boundary case and ≥ 44 for the case without near-field effects. (C) With near-field effects disabled, the final state typically contains multiple domains with different wave vectors. The red line (left scale) shows the percentage of simulation runs that end in a monodomain state and cyan line (right scale) the average domain size as a function of the system size N . (D) Kymograph showing the coherence between adjacent cilia with near-field effects disabled, with the phase kymograph as an inset. Unlike in the case of nonreciprocal coupling (see Fig. 2D), defects between domains with different wave vectors remain after synchronisation (the example shows one defect). (E) Coherence kymograph of the system with near-field effects and periodic boundary conditions. Defects between coherent regions move with the group velocity, but do not get extinguished at the boundaries, again resulting in a long synchronisation time.

in the positive x -direction, the direction of the cilium power stroke. The instantaneous flows, on the other hand, show a periodic structure that follows the movement of metachronal wavefronts.

Although we used a square lattice as an example, the ability of cilia to synchronise is robust against the lattice type and the shape of the arrangement. Similar dynamics is obtained on a hexagonal lattice, as well as on an array with boundaries in the shape of an octagon (Fig. S1).

Role of nonreciprocity and near-field effects. Our model shows strong nonreciprocity in the hydrodynamic interactions between cilia. This can be seen by calculating the shift of beating frequencies caused by hydrodynamic interactions, relative to the unperturbed cilium ($\omega - \omega^{\text{unp}}$). The frequency shifts, averaged over one cycle, are shown in Fig. 5A as a function of the phase difference $\Delta\phi'$ and the relative position of the two cilia, represented by the angle β . Nonreciprocity manifests itself as shifts in the beating frequency of the two interacting cilia. The two cilia can experience dramatically different frequency shifts, with very different magnitudes and functional forms. The degree of this nonreciprocity is highly anisotropic, being much greater in the pumping direction than perpendicular to it (Fig. 5A).

As shown in the section Symmetries, nonreciprocal interactions are not possible when the hydrodynamic interactions are treated in the far-field approximation. In the far-field, the

interaction with a cilium at position β has to be identical to the interaction with a cilium at the opposite position $\beta + \pi$. We demonstrate this by disabling the near-field effects and replacing the off-diagonal elements of the mobility matrix with the approximation given by Eq. (6). The resulting frequency shifts (dashed lines in Fig. 5A) become reciprocal, as they fulfil $\omega_1(\Delta\phi') = \omega_2(-\Delta\phi')$.

To investigate the role of near-field effects in the formation of metachronal waves, we simulated the dynamics of a row of cilia (analogous to the results in Fig. 2) with only far-field interactions. The resulting synchronisation times are significantly longer (orange line in Fig. 5B) than with near-field effects (grey line). In small systems, the scaling with size becomes quadratic (inset in Fig. 5B), whereas we showed them to be linear in the presence of nonreciprocal coupling. However, in larger systems, the synchronisation times saturate, as the final state no longer consists of a uniform metachronal wave. Rather, the system evolves into a long-lived state consisting of multiple domains with distinct wave vectors. An example with two domains, separated by one defect, is shown in Fig. 5D. The mean domain size and the likelihood that the system evolves into a mono-domain metachronal wave are shown in Fig. 5C.

To understand the role of open boundaries in our system, we compared the results to the same system with periodic boundary conditions. Periodic boundary conditions are typical in other hydrodynamic models of ciliary or flagellar synchro-

nisation (11, 12, 26, 31, 32, 34, 38, 50, 53, 54, 62) when there
391 are many cilia present (though with rare exceptions (e.g. 41)),
392 as they ensure that no cilia exist at an open boundary which
393 could cause order to break down – indeed, when such mod-
394 els are subjected to open boundary conditions, they often
395 find only intermittent synchronisation (38). Our results show
396 that introducing periodic boundaries, while preserving the
397 nonreciprocal coupling, strongly increases the synchronisation
398 timescale, which again scales quadratically with the system
399 size (Fig. 5B). The reason why periodic boundary conditions
400 become deleterious to synchronisation can be seen in the co-
401 herence kymograph in Fig. 5E. It shows a number of defects,
402 each propagating with the group velocity v_g , that travel peri-
403 odically across the system, so the system only slowly reaches
404 a coherent state with a single metachronal wave.
405

Discussion. In our study we used a strongly simplified model
406 of a cilium. We replaced the cilium with a single particle
407 moving along a tilted circular trajectory. The tilted trajectory
408 breaks the most important symmetry of the cilium, namely
409 that between the power stroke, when the distance to the
410 surface is larger, and the recovery stroke, when the distance
411 is smaller. This asymmetry is at the core of fluid transport,
412 which does not rely on metachronal coordination, although
413 the metachronal waves can improve the energetic efficiency
414 of cilia (10, 11). At the same time, the driving force and
415 the internal friction are modulated such that they reproduce
416 a power stroke that is faster than the recovery stroke and
417 also reproduce the fore-aft asymmetry that is present in cilia.
418 The modulation of both parameters represents both the cyclic
419 activity of dynein motors and the variations in the shape of the
420 cilium, which is stretched during the power stroke and bent
421 during the recovery stroke. Unlike theoretical models with
422 fewer broken symmetries (35), our model allows the emergence
423 of metachronal waves that are not directly linked to the fluid
424 transport.
425

The numerical solution of the model equations takes into
426 account not only the the far-field hydrodynamics, as in (34),
427 but also the near-field effects that become relevant when the
428 size of a cilium becomes comparable to the distance between
429 adjacent cilia. Near-field effects are definitely important in
430 most ciliary systems that show metachronal coordination. For
431 example, in *Paramecium* the intercilium distance is in the
432 micrometre range, which is several times less than the cilium
433 length (63). In respiratory epithelia the distances are even
434 shorter at fractions of a micrometre (64). On the other hand,
435 in *Volvox* colonies, pairs of flagella (one on each cell) are
436 spaced at a distance comparable to their length and still form
437 metachronal waves (15). The intermediate densities we chose
438 here allow us to take a generic approach that does not depend
439 on fine details of the trajectory, while qualitatively capturing
440 the near-field interactions. We therefore expect that the mag-
441 nitude of near-field effects, as well as interactions in general
442 in our study, is underestimated, and that the underlying prin-
443 ciples can account for significantly faster synchronisation in
444 natural cilia.
445

Our main finding is that the near-field effects can make
446 the coupling nonreciprocal. The nonreciprocity goes beyond
447 the asymmetry discussed in (50), which implies that two cilia
448 tend to synchronise with a phase difference that depends on
449 their relative orientation. The nonreciprocal magnitude of the
450 interaction means that a cilium tends to follow a neighbour
451

on one side and to entrain the neighbour in the opposite di-
452 rection. An easy-to-understand mechanism that contributes
453 to nonreciprocity is that the periodically modulated driving
454 force and internal drag make the cilium more susceptible to
455 hydrodynamic interactions in certain parts of the trajectory,
456 which are in turn closer to some neighbours than the others.
457 The nonreciprocal coupling introduces a third direction in the
458 plane, after the direction of fluid transport and the direction
459 of the preferred metachronal wave, which dictates the propa-
460 gation of order. We therefore refer to it as a group velocity.
461 However, we note that unlike in classical waves in linear media
462 with energy conservation, the group velocity is not related to
463 the phase velocity in a straightforward way (e.g. through a
464 dispersion relation).
465

Nonreciprocal coupling has two major effects on the forma-
466 tion of metachronal waves. First, it produces robust waves
467 in finite systems with open boundaries. While open bound-
468 aries are the standard in real systems, they are detrimental
469 in many models of synchronisation, and also in experimental
470 model systems (51). The majority of theoretical works on
471 cilia synchronisation therefore only investigate systems with
472 periodic boundary conditions. In the presence of nonreciprocal
473 coupling, the situation reverses and boundaries help seed the
474 order which then rapidly spreads across the system. With
475 nonreciprocal interactions, it is actually the periodic boundary
476 conditions that significantly slow down the convergence to
477 an ordered metachronal wave. The second major effect of
478 nonreciprocal coupling is that the timescale of metachronal
479 wave formation scales linearly with linear dimension of the
480 system. This holds in both one and two dimensions, due to
481 the linear spreading of order through the system from a bound-
482 ary. At each system size tested, as long as near-field effects
483 are not suppressed, the system always converges to the same
484 metachronal wavevector regardless of the random initial con-
485 ditions, meaning that the basin of attraction is effectively as
486 large as the phase space of the system. We have demonstrated
487 that suppressing the near-field hydrodynamic interactions (and
488 therefore the nonreciprocal coupling) gives rise to unfavourable
489 synchronisation time scaling and unpredictable final states
490 with long-living defects remaining.
491

Our model does not account for non-hydrodynamic interac-
492 tions which have been shown to be relevant for cilium synchro-
493 nisation, such as steric effects (65) and basal coupling (22).
494 Because it has been shown that hydrodynamic interactions
495 alone are sufficient to achieve synchronisation (66), one can
496 consider these other effects as intercilium coupling to fine-tune
497 the interactions rather than being an absolute requirement.
498 In particular, basal coupling could provide a means to align
499 metachronal waves in order to optimise efficiency (67). Finally,
500 we neglected any inertial effects which are known to be small
501 compared to viscous forces in systems of cilia. Nevertheless,
502 it is still possible that a small inertial effect can be decisive
503 for synchronisation in situations where other effects cancel
504 out (68, 69).
505

Our results leave some open questions that could be ad-
506 dressed in future work. For example, in real biological systems
507 there are a great many sources of noise (70), and at the scale
508 of cilia, noise may be very relevant for synchronisation (60) so
509 future extensions to our model could examine the role of noise
510 in the motion of the cilia. Additionally, we have assumed that
511 all cilia are of identical lengths, but in reality there can be
512

variation in the lengths of cilia, and some studies have found that this can affect synchronisation (71). Similarly, even in healthy humans there are some cilia with structural abnormalities (72), which means that the influence on synchronisation of nonidentical cilia may be significant. Our circular trajectory retains many key features of the stroke of real cilia, but it is possible that some crucial feature is lost in this simplification, so future work could integrate realistic cilium strokes with elongated cilia. This would also enable a more realistic driving engine for the cilia: in our model the cilia have a time-varying driving force that always points along the tangent of the trajectory, but real cilia are driven by creating shear forces between pairs of dynein tubes that make up the internal structure of the cilium (73). It is possible that in the future, artificial or lab-grown cilia may have applications in microfluidic pumping, given the advancing state of the fields of growing artificial lab-on-a-chip cilia (74) and nanoscale artificial cilium production (75), which could offer real-world applications for our work and the future work proposed here.

Materials and Methods

Fluid flow. At the scale of cilia, the behaviour of the fluid flow field \mathbf{u} is well-approximated by the incompressible Stokes equations:

$$\eta \nabla^2 \mathbf{u} - \nabla p = 0, \\ \nabla \cdot \mathbf{u} = 0,$$

where η is the fluid dynamic viscosity and p is the pressure.

The hydrodynamic interactions between two particles are calculated using a modified Rotne-Prager approximation with corrections to account for the no-slip fluid boundary on the surface below the cilium. The Rotne-Prager tensor takes into account terms up to the order $\sim r^{-3}$ and is equivalent to averaging the Green's function (Oseen tensor) over the surfaces of both spheres. To take into account the presence of the no-slip boundary at $z=0$, we use the method of images and replace the free-space Green's function by the Blake tensor (76), defined as

$$\mathbf{M}_{ij}^{\text{Blake}} = \frac{1}{8\pi\eta} \left[\mathbf{G}^S(\mathbf{x}_i - \mathbf{x}_j) - \mathbf{G}^S(\mathbf{x}_i - \bar{\mathbf{x}}_j) + 2z_j^2 \mathbf{G}^D(\mathbf{x}_i - \bar{\mathbf{x}}_j) - 2z_j \mathbf{G}^{SD}(\mathbf{x}_i - \bar{\mathbf{x}}_j) \right], \quad [9]$$

where \mathbf{x}_k is the position of particles k , and $\bar{\mathbf{x}}_k$ is the position of the image of particle k reflected in the no-slip boundary at $z=0$, and where

$$\mathbf{G}_{\alpha\beta}^S(\mathbf{r}) = \frac{\delta_{\alpha\beta}}{r} + \frac{r_\alpha r_\beta}{r^3}, \quad [10]$$

$$\mathbf{G}_{\alpha\beta}^D(\mathbf{r}) = (1 - 2\delta_{\beta z}) \frac{\partial}{\partial r_\beta} \left(\frac{r_\alpha}{r^3} \right), \quad [11]$$

$$\mathbf{G}_{\alpha\beta}^{SD}(\mathbf{r}) = (1 - 2\delta_{\beta z}) \frac{\partial}{\partial r_\beta} G_{\alpha z}^S(\mathbf{r}). \quad [12]$$

The Rotne-Prager tensor corrected for the no-slip boundary follows by including the leading corrections that result from surface-averaging over each sphere. The non-diagonal terms, describing the interaction between two particles $i \neq j$, can be calculated as

$$\mathbf{M}_{ij} = \left(1 + \frac{a^2}{6} \nabla_{\mathbf{x}_i}^2 \right) \left(1 + \frac{a^2}{6} \nabla_{\mathbf{x}_j}^2 \right) \mathbf{M}_{ij}^{\text{Blake}}. \quad [13]$$

Explicit expressions for the elements of the mobility matrix can be found in (77).

Solving equations of motion. The equations of motion as stated in Eq. (5) give a complete description of the system. However, they require the knowledge of the many-particle drag matrix Γ , whereas the Rotne-Prager approximation gives us the mobility matrix $\mathbf{M} = \Gamma^{-1}$. Simulating Eq. (5) directly for N cilia would therefore require

the inversion of a $3N \times 3N$ matrix at each simulation step, in addition to solving a linear equation system with N unknowns.

To accelerate the numerical solution, we therefore rewrite the equations of motion based on the mobility matrix $\mathbf{M}(\phi_i, \phi_j)$ which gives the velocity response at the position of cilium i to a force at cilium j . We can express the force balance and the hydrodynamic equations with the hydrodynamic force \mathbf{F}_i^h acting on the cilium:

$$0 = \mathbf{t}_i \cdot \mathbf{F}_i^h(\{j\}) + F_i^{\text{dr}}(\phi_i) - \Gamma(\phi_i)v_i, \quad [14]$$

$$\mathbf{v}_i = -\mathbf{M}(\phi_i, \phi_i) \cdot \mathbf{F}_i^h - \sum_{j \neq i} \mathbf{M}(\phi_i, \phi_j) \cdot \mathbf{F}_j^h. \quad [15]$$

By multiplying the first equation with \mathbf{t}_i and inserting it into the second, we can derive a coupled set of $3N$ equations which allow us to solve for all hydrodynamic force vectors simultaneously (assuming that $\Gamma(\phi)$ is never zero):

$$\left(\mathbf{M}(\phi_i, \phi_i) + \frac{\mathbf{t}_i \mathbf{t}_i^T}{\Gamma(\phi_i)} \right) \cdot \mathbf{F}_i^h + \sum_{j \neq i} \mathbf{M}(\phi_i, \phi_j) \cdot \mathbf{F}_j^h = -\frac{F_i^{\text{dr}}(\phi_i)}{\Gamma(\phi_i)} \mathbf{t}_i.$$

In the above equation system the first term describing the self-interaction of cilium i is always dominant, whereas the second term describing the hydrodynamic interactions between cilia is weaker and can be treated in a perturbative way. In matrix form the equation is always block-diagonally dominant, which means that it can be solved efficiently using an adapted Successive Over-Relaxation (SOR) algorithm (78) that works on 3×3 blocks rather than individual elements. In the initial time step of the simulation, we use the solution to the purely diagonal matrix equation as the first iteration, but in subsequent step it is more efficient to start iterating with the solution of the previous step. In this way only a very small number of iterations ($N_{\text{it}} = 3$) is required to converge to remarkably good accuracy with a relative error $\varepsilon < 10^{-6}$. Once the hydrodynamic forces have been obtained, they can be substituted back into Eq. (14) to find the cilium speeds v_i , and this can be trivially transformed into the time derivatives of the phases $\dot{\phi}_i$.

Numerical integration. The phase of each cilium is updated using the standard Runge-Kutta method (RK4). Unlike implicit methods, Runge-Kutta algorithms require a single calculation of the hydrodynamic forces at each timestep, which is by far the most computationally demanding simulation step. The timestep used was approximately $0.001 t_0$.

Quantifying synchronisation. To determine whether the entire system has reached a synchronised state, we find the average frequencies of each cilium in a moving window of 50 time periods. We take the standard deviation of these frequencies to be the order parameter of the system.

When considering pairs of cilia, as in Figs. 2C, 3D, and 5D-E, standard deviations were less useful. Instead, the signal coherence was computed using the phases of adjacent pairs of cilia using Welch's method (79), with a moving window in the time domain representing approximately 50 unperturbed cilium cycles. In the 2D case, we instead used the geometric mean of the coherence with all neighbouring cilia.

Uniform phase angle. In Fig. 5 we used a transformed phase difference $\Delta\phi' = \phi'_2 - \phi'_1$. These angles have the property that for a single isolated cilium, ϕ' is constant. The transformed phase can be derived from the original phase angle using

$$\phi'(\phi) = \frac{2\pi}{t_0} \int_0^\phi \frac{1}{\dot{\phi}(\phi'')} d\phi'', \quad [16]$$

where all quantities on the right hand side are for an isolated cilium.

Periodic boundary conditions. When considering the effect of cilium j on cilium i , only the closest instance of j was considered. In simple terms, if j were right next to i , then we would proceed in the same way as if we had no periodic boundaries. However, if j were more than half of the system length away from i , then we would instead consider a copy of j translated by the system length, putting it closer to i . Since the mobility tensor decays quickly along the surface as $1/r^3$, neglecting the distant cilia does not have any effect on the results.

546
547

548
549
550
551
552
553
554
555
556
557
558
559
560
561
562
563

564
565
566
567
568
569
570
571
572
573
574
575
576
577
578
579
580
581

582
583
584
585
586
587
588
589
590
591
592
593
594
595
596

597 **Numerical parameters.** In all simulations, we took the lattice constant
 598 to be $d = 2.5h = 2.5a$, and $b = a/10$. χ was always $\pi/6$ and we
 599 used $A_1 = -0.55$, $A_2 = -0.2$, $B_1 = -0.2$, $B_2 = 0.35$, $C_1 = 0.3$,
 600 $C_2 = -0.4$, $D_1 = -0.1$, and $D_2 = -0.55$. These parameters give
 601 a fast working stroke and a slower recovery stroke which break
 602 the fore-aft symmetry, consistent with the behaviour of real cilia.
 603 The slowest part of the stroke is just before the lowest part of the
 604 recovery stroke, where the cilium would be curling up and the tip
 605 would therefore be travelling at its minimum speed.

606 **ACKNOWLEDGMENTS.** This work has received support from the
 607 Max Planck School Matter to Life and the MaxSynBio Consortium,
 608 which are jointly funded by the Federal Ministry of Education and
 609 Research (BMBF) of Germany, and the Max Planck Society. A.V.
 610 acknowledges support from the Slovenian Research Agency (grant
 611 no. P1-0099)

- 612 1. C Brennen, H Winet, Fluid mechanics of propulsion by cilia and flagella. *Annu. Rev. Fluid
 613 Mech.* **9**, 339–398 (1977).
- 614 2. MV Nachury, DU Mick, Establishing and regulating the composition of cilia for signal transduc-
 615 tion. *Nat. Rev. Mol. Cell Biol.* **20**, 389–405 (2019).
- 616 3. R Faubel, C Westendorf, E Bodenschatz, G Eichele, Cilia-based flow network in the brain
 617 ventricles. *Science* **353**, 176–178 (2016).
- 618 4. A Yaghi, MB Dolovich, Airway epithelial cell cilia and obstructive lung disease. *Cells* **5**, 40
 619 (2016).
- 620 5. V Bhandawat, J Reisert, KW Yau, Signaling by olfactory receptor neurons near threshold.
 621 *Proc. Natl. Acad. Sci. U.S.A.* **107**, 18682–18687 (2010).
- 622 6. A Dasgupta, JD Amack, Cilia in vertebrate left-right patterning. *Phil. Trans. Royal Soc. B: Biol.
 623 Sci.* **371**, 20150410 (2016).
- 624 7. L Prandtl, Aufgaben der Strömungsforschung (lecture delivered at the inauguration of the
 625 Kaiser Wilhelm Institute for Flow Research in Göttingen, 16 July 1925). *Naturwissenschaften*
 626 **14**, 335–338 (1926).
- 627 8. GI Taylor, Analysis of the swimming of microscopic organisms. *Proc. R. Soc. Lond. A* **209**,
 628 447–461 (1951).
- 629 9. R Golestanian, JM Yeomans, N Uchida, Hydrodynamic synchronization at low Reynolds
 630 number. *Soft Matter* **7**, 3074 (2011).
- 631 10. N Osterman, A Vilfan, Finding the ciliary beating pattern with optimal efficiency. *Proc. Natl.
 632 Acad. Sci. U.S.A.* **108**, 15727–15732 (2011).
- 633 11. J Elgeti, G Gompper, Emergence of metachronal waves in cilia arrays. *Proc. Natl. Acad. Sci.
 634 U.S.A.* **110**, 4470–4475 (2013).
- 635 12. C Ringers, et al., Novel analytical tools reveal that local synchronization of cilia coincides with
 636 tissue-scale metachronal waves in zebrafish multiciliated epithelia. *eLife* **12**, e77701 (2023).
- 637 13. D Hickey, A Vilfan, R Golestanian, Ciliary chemosensitivity is enhanced by cilium geometry
 638 and motility. *eLife* **10**, e66322 (2021).
- 639 14. A Funak, et al., *Paramecium* swimming and ciliary beating patterns: a study on four RNA
 640 interference mutations. *Integr. Biol.* **7**, 90–100 (2015).
- 641 15. DR Brumley, M Polin, TJ Pedley, RE Goldstein, Hydrodynamic synchronization and
 642 metachronal waves on the surface of the colonial alga *Volvox carteri*. *Phys. Rev. Lett.* **109**,
 643 268102 (2012).
- 644 16. S Chateau, J Favier, S Poncet, U D'Ortona, Why antiplectic metachronal cilia waves are
 645 optimal to transport bronchial mucus. *Phys. Rev. E* **100**, 791 (2019).
- 646 17. ML Bryon, et al., Metachronal motion across scales: Current challenges and future directions.
 647 *Integr. Comp. Biol.* **61**, 1674–1688 (2021).
- 648 18. EW Knight-Jones, Relations between metachronism and the direction of ciliary beat in metazoa.
 649 *J. Cell Sci.* **3**, 503–521 (1954).
- 650 19. RE Goldstein, M Polin, I Tuval, Noise and synchronization in pairs of beating eukaryotic flagella.
 651 *Phys. Rev. Lett.* **103**, 168103 (2009).
- 652 20. KY Wan, RE Goldstein, Coordinated beating of algal flagella is mediated by basal coupling.
 653 *Proc. Natl. Acad. Sci. U.S.A.* **113**, E2784–E2793 (2016).
- 654 21. G Quaranta, ME Aubin-Tam, D Tam, Hydrodynamics versus intracellular coupling in the
 655 synchronization of eukaryotic flagella. *Phys. Rev. Lett.* **115**, 238101 (2015).
- 656 22. Y Liu, R Claydon, M Polin, DR Brumley, Transitions in synchronization states of model cilia
 657 through basal-connection coupling. *J. Royal Soc. Interface* **15**, 20180450 (2018).
- 658 23. N Narematsu, R Quek, KH Chiam, Y Iwade, Ciliary metachronal wave propagation on the
 659 compliant surface of *Paramecium* cells. *Cytoskeleton* **72**, 633–646 (2015).
- 660 24. M Reichert, H Stark, Synchronization of rotating helices by hydrodynamic interactions. *Eur.
 661 Phys. J. E* **17**, 493–500 (2005).
- 662 25. B Guirao, JF Joanny, Spontaneous creation of macroscopic flow and metachronal waves in an
 663 array of cilia. *Biophys. J.* **92**, 1900–1917 (2007).
- 664 26. T Niedermayer, B Eckhardt, P Lenz, Synchronization, phase locking, and metachronal wave
 665 formation in ciliary chains. *Chaos* **18**, 037128 (2008).
- 666 27. B Qian, H Jiang, DA Gagnon, KS Breuer, TR Powers, Minimal model for synchronization
 667 induced by hydrodynamic interactions. *Phys. Rev. E* **80**, 061919 (2009).
- 668 28. N Uchida, R Golestanian, Hydrodynamic synchronization between objects with cyclic rigid
 669 trajectories. *Eur. Phys. J. E* **35**, 135 (2012).
- 670 29. Y Man, E Kanso, Multisynchrony in Active Microfilaments. *Phys. Rev. Lett.* **125**, 148101
 671 (2020).
- 672 30. A Vilfan, F Jülicher, Hydrodynamic flow patterns and synchronization of beating cilia. *Phys.
 673 Rev. Lett.* **96**, 1–4 (2006).
- 674 31. N Uchida, R Golestanian, Synchronization and collective dynamics in a carpet of microfluidic
 675 rotors. *Phys. Rev. Lett.* **104**, 178103 (2010).
- 676 32. N Uchida, R Golestanian, Synchronization in a carpet of hydrodynamically coupled rotors with
 677 random intrinsic frequency. *Europhys. Lett.* **89**, 50011 (2010).
- 678 33. S Saha, S Ramaswamy, R Golestanian, Pairing, waltzing and scattering of chemotactic active
 679 colloids. *New J. Phys.* **21**, 063006 (2019).
- 680 34. F Meng, RR Bennett, N Uchida, R Golestanian, Conditions for metachronal coordination in
 681 arrays of model cilia. *Proc. Natl. Acad. Sci. U.S.A.* **118** (2021).
- 682 35. AV Kanale, F Ling, H Guo, S Fürthauer, E Kanso, Spontaneous phase coordination and fluid
 683 pumping in model ciliary carpets. *Proc. Natl. Acad. Sci. U.S.A.* **119**, e2214413119 (2022).
- 684 36. N Uchida, R Golestanian, Generic conditions for hydrodynamic synchronization. *Phys. Rev.
 685 Lett.* **106**, 058104 (2011).
- 686 37. A Maestro, et al., Control of synchronization in models of hydrodynamically coupled motile
 687 cilia. *Commun. Phys.* **1**, 1–8 (2018).
- 688 38. C Wollin, H Stark, Metachronal waves in a chain of rowers with hydrodynamic interactions.
 689 *Eur. Phys. J. E* **34**, 42 (2011).
- 690 39. H Guo, L Fauci, M Shelley, E Kanso, Bistability in the synchronization of actuated microfila-
 691 ments. *J. Fluid Mech.* **836**, 304–323 (2018).
- 692 40. B Chakrabarti, D Saintillan, Hydrodynamic synchronization of spontaneously beating filaments.
 693 *Phys. Rev. Lett.* **123**, 208101 (2019).
- 694 41. B Chakrabarti, S Fürthauer, MJ Shelley, A multiscale biophysical model gives quantized
 695 metachronal waves in a lattice of cilia. *Proc. Natl. Acad. Sci. U.S.A.* **119**, e2113539119 (2022).
- 696 42. H Masoud, HA Stone, The reciprocal theorem in fluid dynamics and transport phenomena. *J.
 697 Fluid Mech.* **879**, P1 (2019).
- 698 43. R Soto, R Golestanian, Self-assembly of catalytically active colloidal molecules: Tailoring
 699 activity through surface chemistry. *Phys. Rev. Lett.* **112**, 068301 (2014).
- 700 44. R Soto, R Golestanian, Self-assembly of active colloidal molecules with dynamic function.
 701 *Phys. Rev. E* **91**, 052304 (2015).
- 702 45. J Agudo-Canalejo, R Golestanian, Active phase separation in mixtures of chemically interacting
 703 particles. *Phys. Rev. Lett.* **123**, 018101 (2019).
- 704 46. S Saha, J Agudo-Canalejo, R Golestanian, Scalar active mixtures: The nonreciprocal Cahn-
 705 Hilliard model. *Phys. Rev. X* **10**, 041009 (2020).
- 706 47. SAM Loos, SHL Klapp, Irreversibility, heat and information flows induced by non-reciprocal
 707 interactions. *New J. Phys.* **22**, 123051 (2020).
- 708 48. M Fruchart, R Hanai, PB Littlewood, V Vitelli, Non-reciprocal phase transitions. *Nature* **592**,
 709 363–369 (2021).
- 710 49. S Osat, R Golestanian, Non-reciprocal multifarious self-organization. *Nat. Nanotechnol.* **18**,
 711 79–85 (2023).
- 712 50. A Solovev, BM Friedrich, Synchronization in cilia carpets: multiple metachronal waves are
 713 stable, but one wave dominates. *New J. Phys.* **24**, 013015 (2022).
- 714 51. I Kavre, A Vilfan, D Babic, Hydrodynamic synchronization of autonomously oscillating optically
 715 trapped particles. *Phys. Rev. E* **91**, 031002 (2015).
- 716 52. E Hamilton, N Brut, P Cicuta, The chimera state in colloidal phase oscillators with hydrody-
 717 namic interaction. *Chaos* **27**, 123108 (2017).
- 718 53. B Nasouri, GJ Elfring, Hydrodynamic interactions of cilia on a spherical body. *Phys. Rev. E* **93**,
 719 033111 (2016).
- 720 54. FO Mannan, M Jarvela, K Leiderman, Minimal model of the hydrodynamical coupling of flagella
 721 on a spherical body with application to *Volvox*. *Phys. Rev. E* **102**, 033114 (2020).
- 722 55. KY Wan, et al., Reorganization of complex ciliary flows around regenerating Stentor coeruleus.
 723 *Phil. Trans. Royal Soc. B: Biol. Sci.* **375**, 20190167 (2020).
- 724 56. RR Strathmann, The feeding behavior of planktrophic echinoderm larvae: Mechanisms,
 725 regulation, and rates of suspension-feeding. *J. Exp. Mar. Biol. Ecol.* **6**, 109–160 (1971).
- 726 57. A Vilfan, Generic flow profiles induced by a beating cilium. *Eur. Phys. J. E* **35**, 72 (2012).
- 727 58. GJ Elfring, E Lauga, Hydrodynamic phase locking of swimming microorganisms. *Phys. Rev.
 728 Lett.* **103**, 088101 (2009).
- 729 59. A Solovev, BM Friedrich, Lagrangian mechanics of active systems. *Eur. Phys. J. E* **44**, 49
 730 (2021).
- 731 60. A Solovev, BM Friedrich, Synchronization in cilia carpets and the Kuramoto model with local
 732 coupling: Breakup of global synchronization in the presence of noise. *Chaos* **32**, 013124
 733 (2022).
- 734 61. F Boselli, J Jullien, E Lauga, RE Goldstein, Fluid mechanics of mosaic ciliated tissues. *Phys.
 735 Rev. Lett.* **127**, 198102 (2021).
- 736 62. A Ghorbani, A Najafi, Symplectic and antiplectic waves in an array of beating cilia attached to
 737 a closed body. *Phys. Rev. E* **95**, 052412 (2017).
- 738 63. K Bouhouche, et al., *Paramecium*, a model to study ciliary beating and ciliogenesis: Insights
 739 from cutting-edge approaches. *Front. Cell Dev. Biol.* **10**, 847908 (2022).
- 740 64. MA Sleigh, JR Blake, N Liron, The propulsion of mucus by cilia. *Am. Rev. Respir. Dis.* **137**,
 741 726–741 (1988).
- 742 65. R Chelakkot, M Fagan, A Gopinath, Synchronized oscillations, traveling waves, and jammed
 743 clusters induced by steric interactions in active filament arrays. *Soft Matter* **17**, 1091–1104
 744 (2021).
- 745 66. DR Brumley, KY Wan, M Polin, RE Goldstein, Flagellar synchronization through direct hydro-
 746 dynamic interactions. *eLife* **3**, e02750 (2014).
- 747 67. AWJ Soh, et al., Intracellular connections between basal bodies promote the coordinated
 748 behavior of motile cilia. *Mol. Biol. Cell* **33**, br18 (2022).
- 749 68. M Theers, RG Winkler, Synchronization of rigid microrotors by time-dependent hydrodynamic
 750 interactions. *Phys. Rev. E* **88**, 023012 (2013).
- 751 69. D Wei, PG Dehnavi, ME Aubin-Tam, D Tam, Measurements of the unsteady flow field around
 752 beating cilia. *J. Fluid Mech.* **915**, A70 (2021).
- 753 70. W Gilpin, MS Bull, M Prakash, The multiscale physics of cilia and flagella. *Nat. Rev. Phys.* **2**,
 754 74–88 (2020).
- 755 71. M Bottier, KA Thomas, SK Dutcher, PV Bayly, How does cilium length affect beating? *Biophys.
 756 J.* **116**, 1292–1304 (2019).
- 757 72. F Verra, et al., Ciliary abnormalities in bronchial epithelium of smokers, ex-smokers, and
 758 nonsmokers. *Am. J. Respir. Crit. Care Med.* **151** (2013).
- 759 73. A Horani, TW Ferkol, Advances in the genetics of primary ciliary dyskinesia. *Chest* **154**,
 760

- 645–652 (2018).
74. JC Nawroth, et al., Stem cell-based lung-on-chips: The best of both worlds? *Adv. Drug Deliv. Rev.* **140**, 12–32 (2019).
75. JMJ den Toonder, PR Onck, Microfluidic manipulation with artificial/bioinspired cilia. *Trends Biotechnol.* **31**, 85–91 (2013).
76. JR Blake, A note on the image system for a Stokeslet in a no-slip boundary. *Proc. Camb. Phil. Soc.* **70**, 303–310 (1971).
77. M Vilfan, et al., Self-assembled artificial cilia. *Proc. Natl. Acad. Sci. U.S.A.* **107**, 1844–1847 (2010).
78. DM Young, *Iterative Solution of Large Linear Systems*. (Academic Press, Orlando, FL), (1971).
79. P Welch, The use of fast Fourier transform for the estimation of power spectra: A method based on time averaging over short, modified periodograms. *IEEE Trans. Audio Electroacoust.* **15**, 70–73 (1967).

DRAFT